Smart Structures and Systems, Vol. 6, No. 7 (2010) 867-887
DOI: http://dx.doi.org/10.12989/sss.2010.6.7.867

A dragonfly inspired flapping wing actuated by electro active polymers

Sujoy Mukherjee and Ranjan Ganguli*

Department of Aerospace Engineering, Indian Institute of Science, Bangalore-560012, India

(Received July 7, 2009, Accepted November 18, 2009)

Abstract. An energy-based variational approach is used for structural dynamic modeling of the IPMC (Ionic Polymer Metal Composites) flapping wing. Dynamic characteristics of the wing are analyzed using numerical simulations. Starting with the initial design, critical parameters which have influence on the performance of the wing are identified through parametric studies. An optimization study is performed to obtain improved flapping actuation of the IPMC wing. It is shown that the optimization algorithm leads to a flapping wing with dimensions similar to the dragonfly *Aeshna Multicolor* wing. An unsteady aerodynamic model based on modified strip theory is used to obtain the aerodynamic forces. It is found that the IPMC wing generates sufficient lift to support its own weight and carry a small payload. It is therefore a potential candidate for flapping wing of micro air vehicles.

Keywords: ionic polymer metal composites; dynamics; flapping wing; optimization; unsteady aerodynamics; micro air vehicles.

1. Introduction

Research interest on micro air vehicles (MAVs) has been growing because they have a large number of potential military and commercial applications (Pines and Bohorquez 2006). Many researchers have focused on fixed wings to provide lift for these tiny aircraft (Grasmeyer and Keennon 2001, Cosyn and Vierendeels 2007). The potential applications of current fixed wing MAVs are limited due to maneuver constraints, incapability to hover and stall at low speeds. Rotary wing MAVs have significant advantage over fixed wing vehicles in several aspects such as reliable operation over a wide range of operating conditions including the hovering and maneuvering capabilities required to remain stationary or in motion constrained environments (Nelson and Koratkar 2005, Bohorquez *et al.* 2003, Hein and Chopra 2007, Sirohi *et al.* 2007, Kim and Koratkar 2005). However, the rotary wing MAV configurations suffer from low figure of merit, high power consumption and significant noise signatures. Nature provides flapping flyers such as birds and insects which represent a very successful design for intelligent MAVs with much better performance than conventional wings and rotors in terms of hovering capability, maneuverability, acoustic signature, specific power requirement etc. (Shyy *et al.* 1999). Lightweight, flexible and adaptive/morphing wing structures make an important contribution to the overall performance of a flapping wing MAV. Thus, MAV flapping wing design represents one of the major challenges to efficient flight in the low Reynolds-number regime.

*Corresponding Author, Professor, E-mail: ganguli@aero.iisc.ernet.in

Biomimetic flapping wing mechanisms are used for a deeper understanding of flapping flight (Taracio *et al.* 2005, Okamoto and Azuma 2005, Ramasamy and Leishman 2006). Yamamoto and Isogai (2005) developed a mechanical flapping wing apparatus that dynamically simulates the tandem wing configuration of a dragonfly in hovering flight. The flapping and feathering motion are induced by electric sliders and stepping motors, respectively. Their investigations showed that, in hovering flight, there is only a small interaction between the flows over the fore- and hindwings. In another study, McIntosh *et al.* (2006) designed a flapping wing mechanism, inspired from the wing motion of the hummingbird and hovering insects, is driven by a small DC motor. Here, flapping motion of the wing was generated by a simple four-bar mechanism and feathering motion was generated by cam-follower system. In a recent study, Singh and Chopra (2008) have investigated the aeroelastic effects associated with the lightweight and highly flexible wing using a biomimetic flapping mechanism. The desired flapping and pitching motion was generated by a brushless motor, the speed of which was controlled by a sensorless speed controller in combination with a precision pulse generator. Currently, flapping wing mechanisms rely on pneumatic and motor-driven flapping actuators which lead to high weight and system-complexity (Park *et al.* 2005a). Moreover, natural flapping flyers generate lift and thrust using complex wingbeat kinematics which can not be easily mimicked with these conventional actuators. Smart materials are being considered for various engineering applications (Carrion and Spencer 2008, Casciati and van der Eijk 2008, Liu 2008, Ying *et al*. 2009). Piezoelectric materials are widely used in smart structures as sensors and actuators (Manna *et al.* 2009, Park *et al.* 2005b). Several researchers have suggested piezoceramics for actuating the motion of flapping wings (Cox *et al.* 2002). However, such concepts suffer from high weight penalty, high voltage demand and low actuation authority problems.

Ionic polymer metal composites (IPMCs) are a relatively new type of smart material that belongs to the family of Electroactive Polymers (EAP) (Tiwari *et al.* 2008). The similarity in behavior of these materials to biological muscles acquired them the moniker “artificial muscles” (Bar-Cohen 2004). Interesting properties, such as softness, lightness (1-2.5 g cm^{-3}), fast reaction speed (μs to s), large bending displacement (>10%), and low activation voltage (1-7 volt), make IPMCs promising candidates for the design of a flapping wing (Shahinpoor *et al.* 1998). Park *et al.* (2005a) designed a flapping wing actuated by IPMC but they used static modeling method for the simulation of the wing. Lee *et al.* (2006) improved the performance of the IPMC flapping actuator in terms of solvent loss characteristics and actuation force. They transferred the bending motion created by IPMC to a flapping motion through a rack and pinion system. However, their experimental investigation indicates that the actuator is useful at low frequency. In recent years, the modeling of IPMC actuators has reached a higher level of maturity. Buechler and Leo (2007) presented an energy-based method for modeling IPMC structures at high frequency range (0.1-500 Hz) which includes the typical flapping frequency of the natural flyers. With the availability of such models, feasibility and design optimization studies for an IPMC flapping wing actuator have become possible.

In order to analyze the feasibility of IPMC flapping wing configurations, both the structural modeling and aerodynamic modeling aspects are necessary. Aerodynamic models used for the flapping wing flight can be broadly classified into quasi-steady models and unsteady models. The quasi-steady models assume low flapping frequencies so that shed wake effects are negligible (Betteridge and Archer 1974). In the unsteady models, unsteady aerodynamic characteristics are accounted for by the unsteady wake effects (DeLaurier 1993). Selected researchers have used computational fluid dynamics (CFD) to simulate the flapping flight (Wang 2000, Wu and Sun 2004). CFD methods provide a clear picture of the flow by solving the incompressible form of the Navier-Stokes equations. However, CFD simulations are computationally intensive. DeLaurier (1993) proposed an unsteady aerodynamic model based on modified strip theory. The aerodynamic model makes it possible to estimate the aerodynamic performances of harmonically flapping wings in the phase of preliminary design and development (Ke *et al*. 2008). Various aerodynamic effects can be considered in this model such as camber effect, partial leading edge suction effect, viscous effect, unsteady wake effect and dynamic stall model of pitching motion. Therefore, the DeLaurier model is useful for estimating the lift generated by a flapping wing.

In this paper, structural modeling of an IPMC flapping wing is done using variational principle. Dynamic analysis of the wing is performed using numerical simulations. Parametric studies are done to identify the key design variables and their effect on the performance of the wing. An optimization study is performed to achieve improved performance of the IPMC flapping wing. Finally, aerodynamic forces generated by the flapping wing are obtained and feasibility of the IPMC flapping wing concept is shown.

2. Structural model

Schematic diagram of the wing geometry used for the structural modeling is shown in Fig. 1. The flapping wing is fixed at the root and has a rectangular cross-section.

Governing equations are derived using Hamilton's principle, which states

$$\int_{t_1}^{t_2}(\delta\mathcal{T}-\delta\mathcal{V}+\delta\mathcal{W}^{ext})dt = 0 \tag{1}$$

Here, $\delta\mathcal{T}$ is the variation in kinetic energy, $\delta\mathcal{V}$ is the variation in potential energy and $\delta\mathcal{W}^{ext}$ is the variation in work done by external force. The variation in kinetic energy, potential energy and external work done can be expressed as (Buechler and Leo 2007)

$$\delta\mathcal{T} = \delta\underline{A}'\left(\int_{V_{ol}} -\rho\underline{\Phi}_u\underline{\Phi}_u'\, dV_{ol}\right)\ddot{\underline{A}} \tag{2}$$

$$\delta\mathcal{V}_{se} = \delta\underline{A}'\left[\int_{V_{ol}}(L_u\underline{\Phi}_u')'\mathbf{c}^{\mathbf{D}}(j\omega)(L_u\underline{\Phi}_u')dV_{ol}\right]\underline{A} \tag{3}$$

$$\delta\mathcal{V}_{couple} = -\delta\underline{A}'\left[\int_{V_{ol}}(L_u\underline{\Phi}_u')'\mathbf{h}(j\omega)\underline{\Phi}_D'\, dV_{ol}\right]\underline{q}-\delta\underline{q}'\left[\int_{V_{ol}}\underline{\Phi}_D\mathbf{h}'(j\omega)(L_u\underline{\Phi}_u')dV_{ol}\right]\underline{A} \tag{4}$$

$$\delta\mathcal{V}_{dielectric} = \delta\underline{q}'\left[\int_{V_{ol}}\underline{\Phi}_D'\,\boldsymbol{\varepsilon}^{\mathbf{T}^{-1}}(j\omega)\underline{\Phi}_D dV_{ol}\right]\underline{q} \tag{5}$$

$$\delta\mathcal{W}^{ext} = \delta\underline{A}'\underline{\Phi}_u'\underline{f}' + \delta\underline{q}'\underline{v}' \tag{6}$$

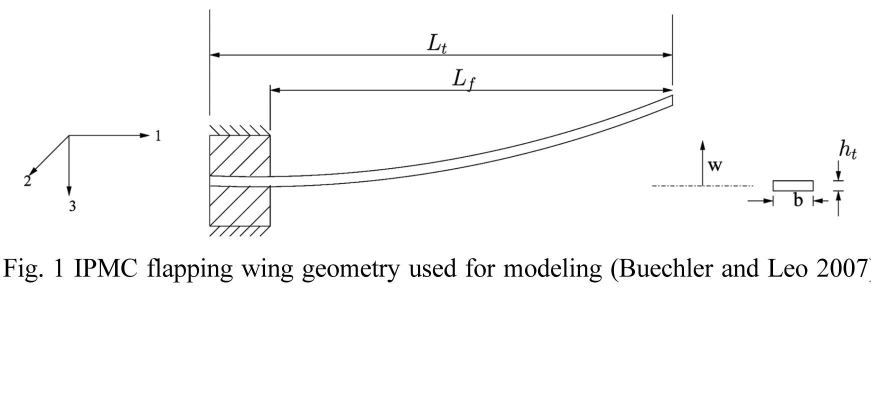

Fig. 1 IPMC flapping wing geometry used for modeling (Buechler and Leo 2007)

The following fundamental assumptions are made for the analysis:
a) Displacements are only in X_3 (flapping) direction,
b) Dielectric permittivity ε_{33} is considered in the analysis, the flapping wing is long and slender therefore Euler-Bernoulli small deflection assumptions are valid,
c) Mode shapes of an uncoupled beam are assumed to be good approximations for the shape functions,
d) One electrode is assumed on each side,
e) Electric displacement is assumed to be constant, and
f) All the charge is assumed to be present on the surface.

Considering all the assumptions and applying Hamilton's principle, the resulting second order differential equations in the frequency domain can be written in a matrix form (Buechler and Leo 2007)

$$\begin{bmatrix} -\mathbf{M}_s\omega^2 + \mathbf{K}_s(j\omega) & \underline{\Psi}(j\omega) \\ \underline{\Psi}'(j\omega) & \mathbf{C}^{-1}(j\omega) \end{bmatrix} \begin{Bmatrix} \underline{A}(j\omega) \\ \underline{q}(j\omega) \end{Bmatrix} = \begin{Bmatrix} \Phi_u{}'\underline{f}(j\omega) \\ \underline{v}'(j\omega) \end{Bmatrix} \tag{7}$$

Mathematical expressions of the above mentioned elements pertaining to the IPMC flapping wing structure, as shown in Fig. 1, are given as

$$C^{-1} = \frac{h_t}{\varepsilon_{33}^T b L_t}$$

$$M_{nn} = \rho b h_t L_f$$

$$K_{nn} = \frac{1}{12} c_{11}^D b h_t^3 L_f \beta_n^4$$

$$\Psi_{n1} = -h_{13}\frac{h_t^2}{2L_t}\int_0^{L_f}\Phi_{un,xx}(x)dx$$

$$\Phi_{un} = \cosh(\beta_n X_1) - \cos(\beta_n X_1) - \sigma_n[\sinh(\beta_n X_1) - \sin(\beta_n X_1)]$$

$$\beta_n^4 = \frac{\rho A \omega_n^2}{EI}$$

$$\sigma_n = \frac{\cosh(\beta_n L_f) + \cos(\beta_n L_f)}{\sinh(\beta_n L_f) + \sin(\beta_n L_f)} \tag{8}$$

Eq. (7) is solved for the generalized coordinates through matrix inversion. In turn, deflection shape of the flapping wing can be determined due to a voltage input. The full details of the IPMC structural model are given in the paper by Buechler and Leo (2007).

3. Aerodynamic model

The aerodynamic model is based on the modified strip theory as proposed by DeLaurier (1993), in which the aerodynamic forces of the flapping wing are obtained by integrating the sectional aerodynamic forces calculated in each section. In this unsteady aerodynamic model, the kinematics for a section of the wing is represented by a plunging velocity $\dot{h}$ and a pitch angle of the chord $\dot{\theta}$ relative to the free stream velocity, as shown in Fig. 2.

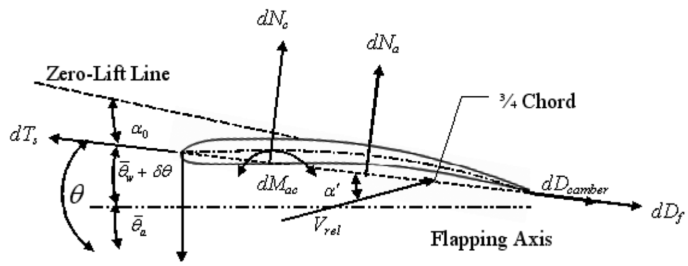

Fig. 2 Aerodynamic forces and motion variables of a wing section (DeLaurier 1993)

The local parameters determining the forces includes the section's geometry, relative angle of attack at the ¾-chord location, pitch rates and the dynamic pressure at the ¼-chord location. The aerodynamic forces acting on each section of the wing are divided into the normal force dN, and the chordwise force, dF_X. The components of the normal force are: (i) dN_c, a circulatory force normal to the chord at the ¼-chord location and (ii) dN_a, an apparent-mass force normal to the chord at the ½-chord location. The expressions for the normal force components are as follows

$$dN_c = \frac{\rho_{air} UV}{2} C_n c dy \tag{9}$$

$$dN_a = \frac{\rho_{air} \pi c^2}{4} \dot{\upsilon}_2 dy \tag{10}$$

Therefore, the section's total attached flow normal force is

$$dN = dN_c + dN_a \tag{11}$$

The components of the chordwise force are: (i) dT_s, a chordwise leading edge suction force, (ii) dD_{camber}, a chordwise drag due to camber, and (iii) dD_f, a chordwise drag due to skin friction. The expressions for the chordwise force components are as follows

$$dT_s = \eta_s 2\pi\left(\alpha' + \bar{\theta}_a - \frac{c\dot{\theta}}{4U}\right)^2 \frac{\rho_{air} UV}{2} c dy \tag{12}$$

$$dD_{camber} = -2\pi\alpha_0(\alpha' + \bar{\theta}_a + \bar{\theta}_w)\frac{\rho_{air} UV}{2} c dy \tag{13}$$

$$dD_f = (C_d)_f \frac{\rho_{air} V_x^2}{2} c dy \tag{14}$$

Thus, the total chordwise force is

$$dF_X = dT_s - dD_{camber} - dD_f \tag{15}$$

The equations for the segment's instantaneous lift dL and thrust dT are

$$dL = dN \cos\theta + dF_X \sin\theta \tag{16}$$

$$dT = dF_X \cos\theta - dN \sin\theta \tag{17}$$

These may be integrated along the span to give the whole wing's instantaneous lift and thrust

$$L(t) = 2\int_0^{\frac{b}{2}} \cos\gamma dL \tag{18}$$

$$T(t) = 2\int_0^{\frac{b}{2}} dT \tag{19}$$

where $\gamma(t)$ is the section's dihedral angle at that instant in the flapping cycle.

The wing's average lift and thrust are obtained by integrating $L(t)$ and $T(t)$ over the cycle. Integrating with respect to cycle angle, ϕ, instead of time, t, where

$$\phi = \omega t \tag{20}$$

so that the average lift and thrust are expressed as

$$\bar{L} = \frac{1}{2\pi}\int_0^{2\pi} L(\phi)d\phi \tag{21}$$

$$\bar{T} = \frac{1}{2\pi}\int_0^{2\pi} T(\phi)d\phi \tag{22}$$

The complete details of the aerodynamic model are given by DeLaurier (1993).

4. Dynamic analysis of the baseline flapping wing

Dragonfly wing size shows substantial variations among the different species. The dragonfly wingspan may vary from 2.63 cm to 6.70 cm due to demographical reasons (Azuma *et al.* 1985, Wakeling and Ellington 1997). The length and width of the flapping wing is taken as 5 cm and 1.2 cm, respectively, which represent typical values for the dragonfly wing. Akle *et al.* (2006) showed that the average thickness of the IPMCs which were manufactured was 0.02 cm. However, thickness of an IPMC can be increased by increasing the thickness of its constituent layers such as ionic polymer membrane layer, upper and lower electrode layers. In this case, thickness of the wing is taken as 0.02 cm in order to keep the mass of the wing as low as possible. Density of the IPMC wing is considered to be 2 g cm^{-3} (Shahinpoor *et al.* 1998). Results in this section are for the 5 cm × 1.2 cm × 0.02 cm IPMC flapping wing, which is called the baseline configuration.

Here the forcing function is assumed to be harmonic, which will essentially flap the wing. Material properties of IPMCs exhibit strong frequency dependence. Fig. 3 shows the frequency dependence of the strain coefficient which can be mathematically expressed as

$$d(s) = -216\frac{s+15}{(s+0.6)(s+14)(s+11000)}\frac{m}{V} \tag{23}$$

It can be seen from Fig. 3 that the strain coefficient is in good agreement with the results presented by Buechler and Leo (2007), thus verifying the implementation of IPMC model. The magnitude of the strain coefficient decreases as frequency increases. However, even with this decrease, the strain coefficients are much higher than those obtained by most other smart materials such as piezoelectric materials. Therefore, the dynamic response of a flapping wing varies at different frequencies. Fig. 4 shows the tip deflection variations of the flapping wing when different voltages at different frequencies are applied. It

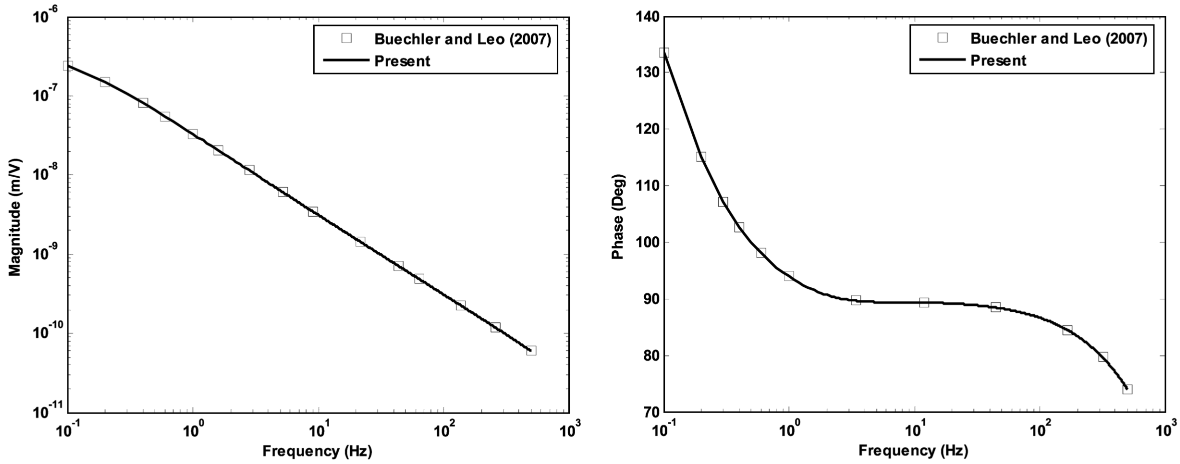

(a) (b)

Fig. 3 Dependence of strain coefficient on frequency

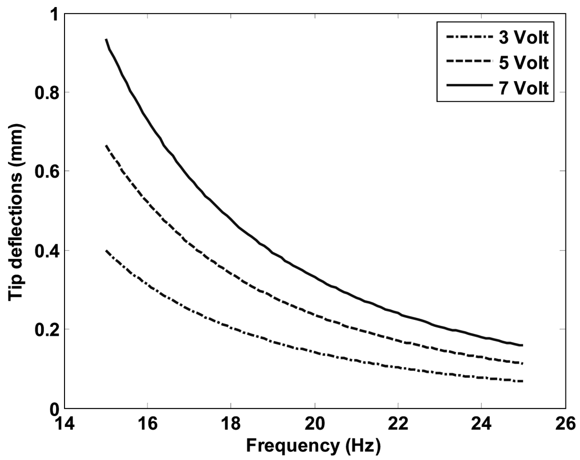

Fig. 4 Tip deflection of IPMC flapping wing due to application of different voltages

can be seen from Fig. 4 that tip deflection decreases with the increase of actuation frequency. This occurs because the magnitude of the strain coefficient decreases with increasing frequency. The strain coefficient represents the electromechanical coupling in terms of the strain induced at the wing surface when an electric field is applied perpendicular to the wing.

Wingbeat flapping frequency of larger insects, such as the hawkmoth *Manduca Sexta*, is 26 Hz, which is very low as compared to the smaller insects, such as blow fly *Calliphora*, which flap their wings at 150 Hz (Deng *et al.* 2006, Willmott and Ellington 1997). Therefore, insects show a scaling effect of the wingbeat frequency with their size of the body. Flapping frequency of dragonfly wing is 32 Hz (Zeng *et al.* 1996) but tip deflection of the IPMC flapping wing is very low at this particular frequency. In order to trade-off between the tip deflection and flapping frequency, tip deflection at 15 Hz is considered for the IPMC flapping wing. Deflected wing shapes for different applied voltages, but at a particular frequency of 15 Hz, which is close to half of the dragonfly wingbeat frequency, is shown in Fig. 5. A flapping angle of 1.27^0 is obtained at 7 volt. However, we will show later in this paper that

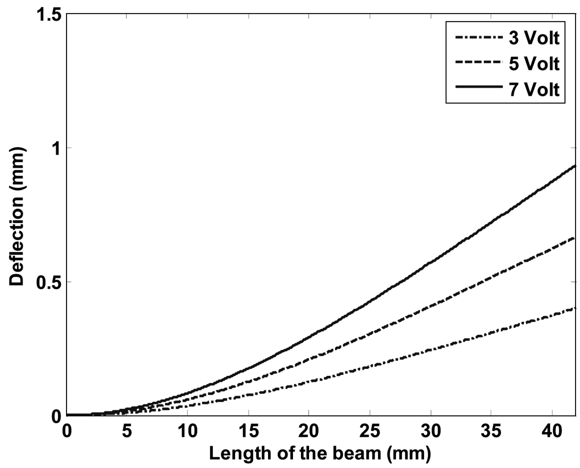

Fig. 5 Deflection shape of the IPMC flapping wing due to application of different voltages

much higher flapping angles are possible by appropriate tailoring of the IPMC wing using mathematical optimization methods.

5. Parametric studies

A particular combination of geometric parameters, such as length, width and thickness, defines the wing geometry. The effects of the variation of geometric parameters on the performance of the IPMC flapping wing are studied in this section. This parametric study is important because critical design variables can be identified for improving the performance of the flapping wing.

5.1 Effect of length

The effects of the variation of length and frequency on the flapping wing performance are shown in Fig. 6 at different voltages. For any given voltage, peak value of tip deflection of a wing geometry is dictated by its length and occurs at a particular frequency. It can be seen from Fig. 7 that the peak value of tip deflections increases with increase of the wing length at different input voltages. Fig. 8 shows that flapping frequency decreases with the increase of the wing length at different input voltages. Flapping frequency at which maximum tip deflection occurs is the same for a wing geometry for all input voltages. However, mass of the flapping wing increases with an increase of the wing length.

5.2 Effect of width

The effects of the variation of width on the flapping wing performance are shown in Fig. 9 at different voltages. Fig. 10 shows that variation of wing width has no effect on maximum tip deflection for a particular input voltage where as magnitude of maximum tip deflection varies when different voltages are applied. Moreover, flapping frequency at which the maximum tip deflection occurs does not change with the variation of wing width at different input voltages as shown in Fig. 11. The only effect in this case is the increase of mass with the increase of the wing width.

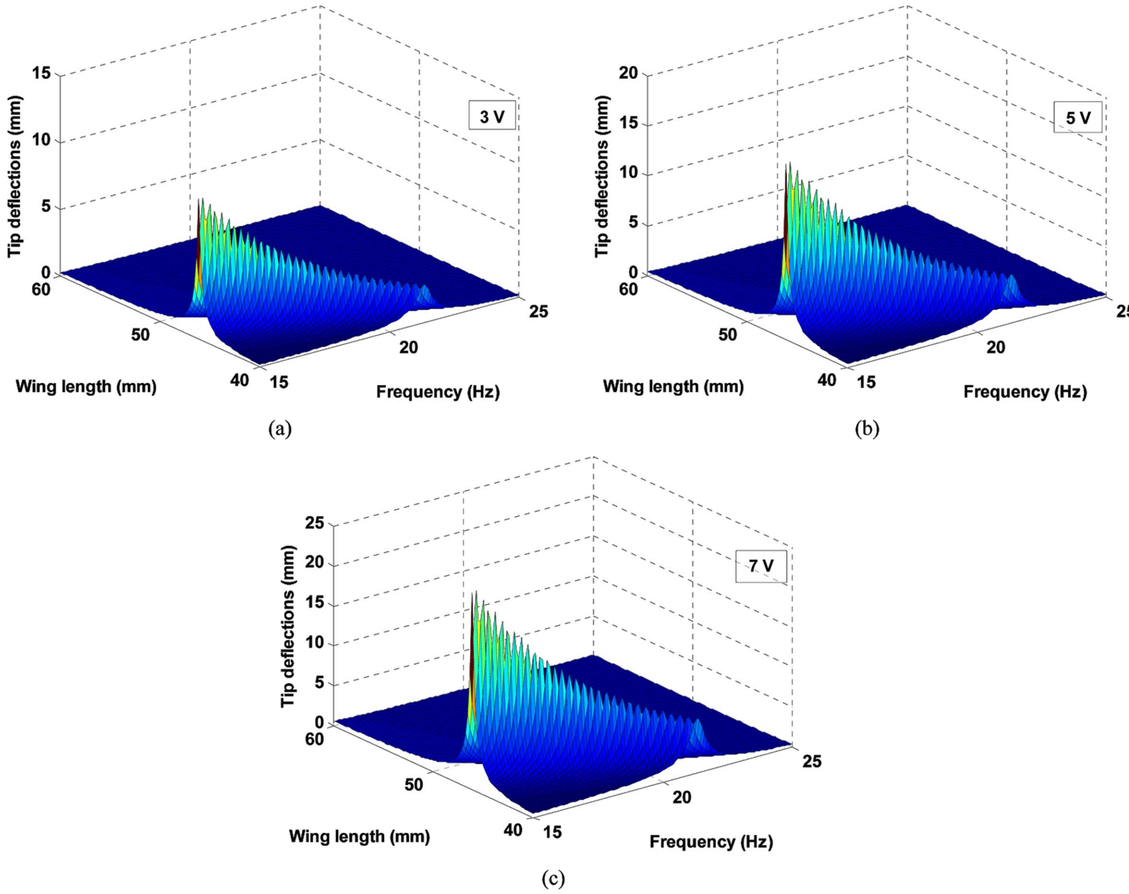

Fig. 6 Effects of the variation of length on the IPMC flapping wing performance at different applied voltages

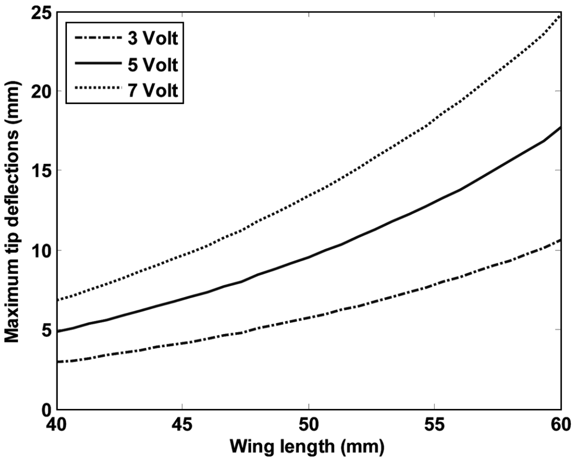

Fig. 7 Effect of the flapping wing length variation on maximum tip deflections at different applied voltages

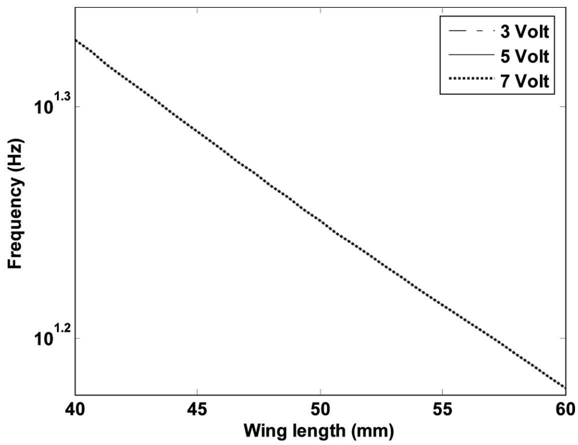

Fig. 8 Effect of the flapping wing length variation on flapping frequencies at different applied voltages

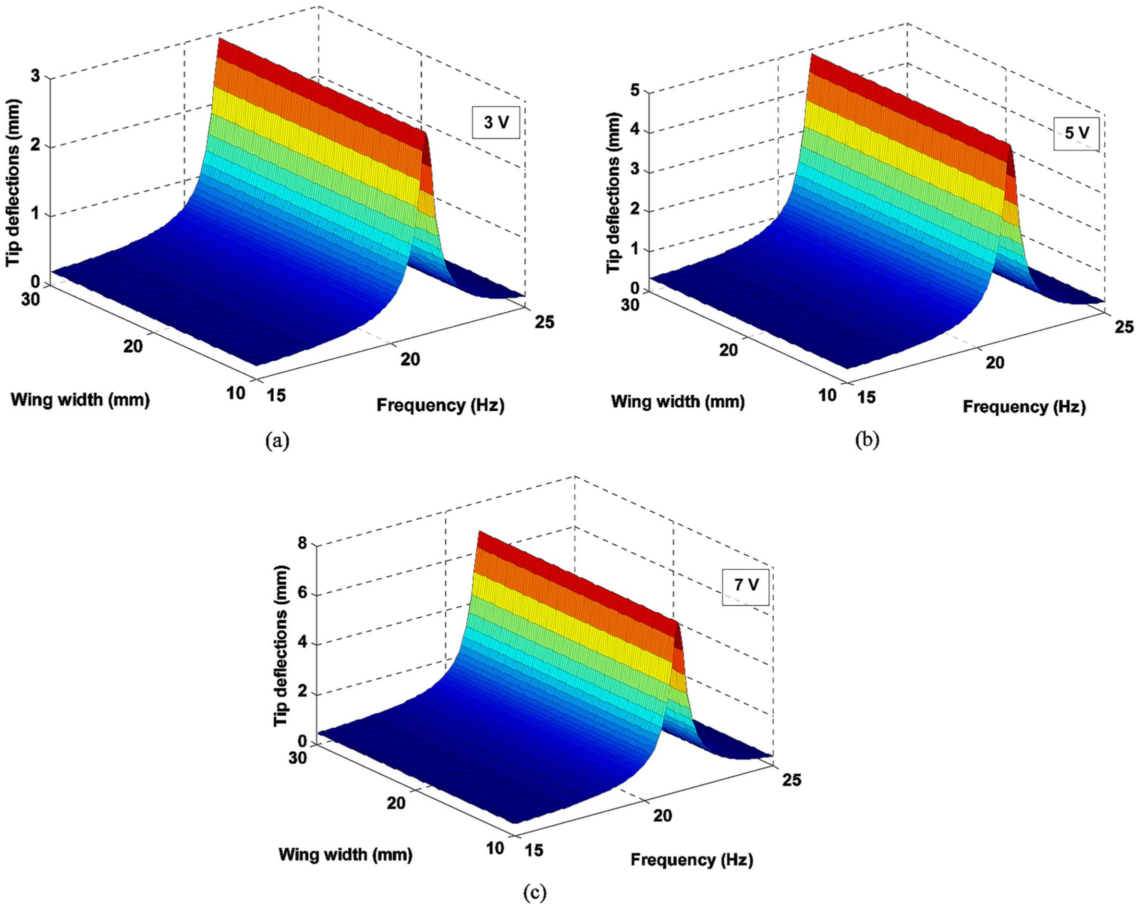

Fig. 9 Effects of the variation of width on the IPMC flapping wing performance at different applied voltges

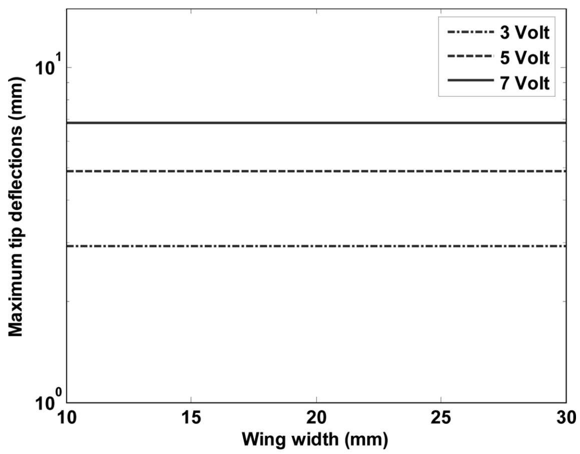

Fig. 10 Effect of the flapping wing width variation on maximum tip deflections at different applied voltages

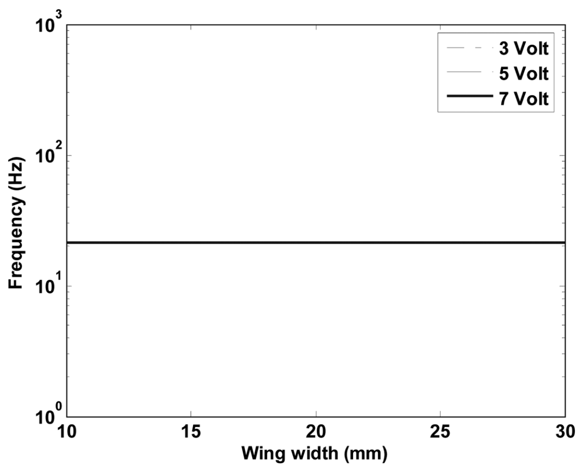

Fig. 11 Effect of the flapping wing width variation on flapping frequencies at different voltages

5.3 Effect of thickness

Finally, the effects of the variation of thickness on the flapping wing performance are shown in Fig. 12 at different voltages. In this case, peak value of tip deflections decreases with increase of the wing thickness at different input voltages as shown in Fig. 13. However, mass of the wing increases with the

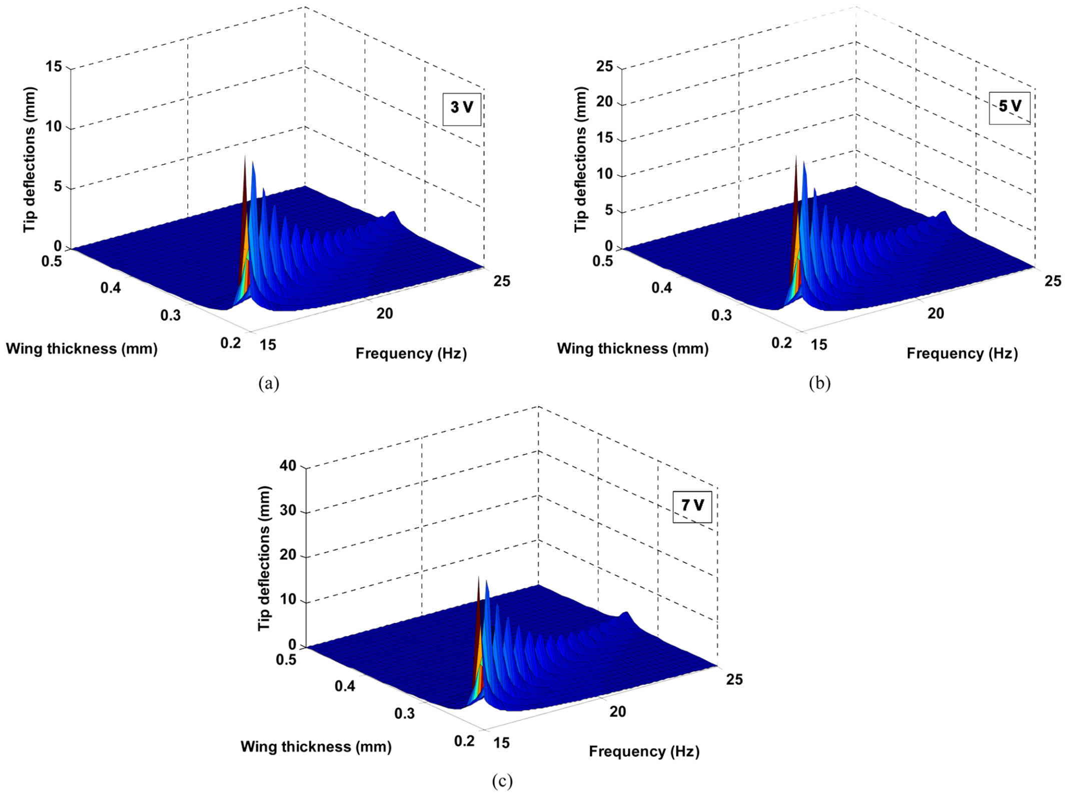

Fig. 12 Effects of the variation of thickness on the IPMC flapping wing performance at different applied voltages

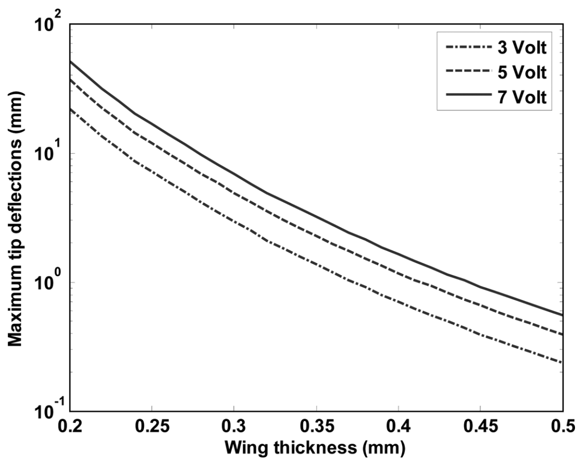

Fig. 13 Effect of the flapping wing thickness variation on maximum tip deflections at different applied voltages

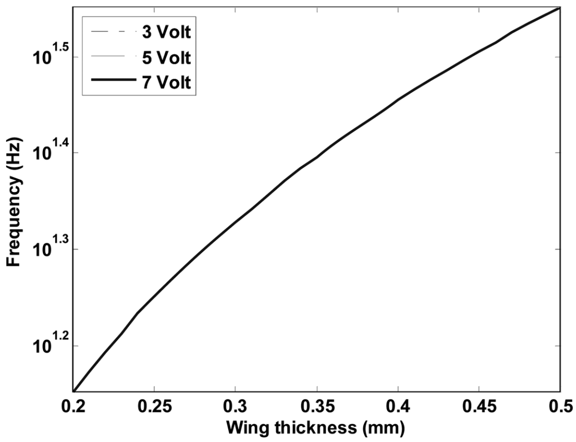

Fig. 14 Effect of the flapping wing thickness variation on flapping frequencies at different applied voltages

increase of the wing thickness. On the other hand, Fig. 14 shows that flapping frequency increases with the increase of the wing thickness at different input voltages. Flapping frequency at which maximum tip deflection occurs is same for a flapping wing geometry for all input voltages.

To summarize, the effects of the variation of length and thickness are opposite to each other while variation of width has no direct effect on the flapping wing performance. However, all three variables affect the mass. The average flapping angle of dragonfly wing is 34^0 as measured by Zeng *et al.* (1996), while the flapping angle obtained with the baseline IPMC flapping wing is less than 2^0 for 7 volt. Therefore, an optimization study is performed to obtain improved flapping wing performance. We seek to maximize the actuation authority of the IPMC flapping wing.

6. Optimization

To perform the optimization study, the problem of maximizing actuation authority is defined in a standard form of the general optimization problem as shown in Eq. (23)

$$\begin{gathered} \text{Maximize } w_{tip}(\mathrm{x}) \\ \text{where } \mathrm{x}=\{L_t, b, h_t\} \\ \text{subject to:} \\ 0 \le (mass)_{actuator} \le (mass)_{baseline} \\ (L_t)_l \le L_t \le (L_t)_u \\ (b)_l \le b \le (b)_u \\ (h_t)_l \le h_t \le (h_t)_u \end{gathered} \tag{24}$$

Here, constraint on the mass of the flapping wing is imposed and mass of the baseline wing, as shown in Table 1, has been set as upper limit. There should be no mass penalty to maximize the actuation authority and therefore we pose the problem as a constrained nonlinear optimization problem with appropriate move limits. The numerical results are obtained at 7 volt.

Table 1 Baseline and optimal values for design optimization

Parameter	Length (mm)	Width (mm)	Thickness (mm)	Maximum tip deflections (mm)	Mass (mg)
Baseline values	50	12	0.2	0.93	240
Optimal values	40	10	0.3	6.84	240

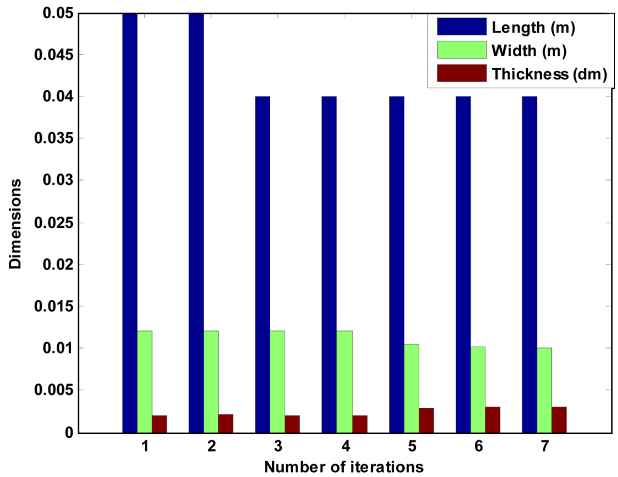

Fig. 15 Iteration history of design variables

The sequential quadratic programming (SQP) algorithm is used to perform the design optimization (Arora 2004). SQP is a gradient based optimization method for nonlinear constrained optimization problem. The gradients are calculated using the finite difference method. Fig. 15 shows the iteration history of the design variables. It can be seen from the Fig. 15 that iteration starts with the baseline values for the length, width and thickness of the wing and optimal values are obtained after seven iterations. The optimizer reduces the length and the width and increases the thickness of the wing. The baseline and optimal values of the IPMC wing are given in Table 1. We see a large increase in maximum tip deflection for the optimal flapping wing.

7. Optimal flapping wing

The optimum values for the length, width and the thickness of the IPMC flapping wing were found to be 40 mm, 10 mm and 0.3 mm, respectively. After searching the literature we found that the optimum length and width of the IPMC wing are typical average values for the wing of the dragonfly *Aeshna Multicolor* as reported by Combes and Daniel (2003). They measured the flexural stiffness variation of the dragonfly *Aeshna Multicolor* wings and approximated the variation by an exponential decline as shown in Fig. 16 and which can be written as

$$EI(X_1) = c.\exp^{aX_1}$$

$$\overline{EI} = \frac{1}{L}\int_0^L EI(X_1)dx \tag{25}$$

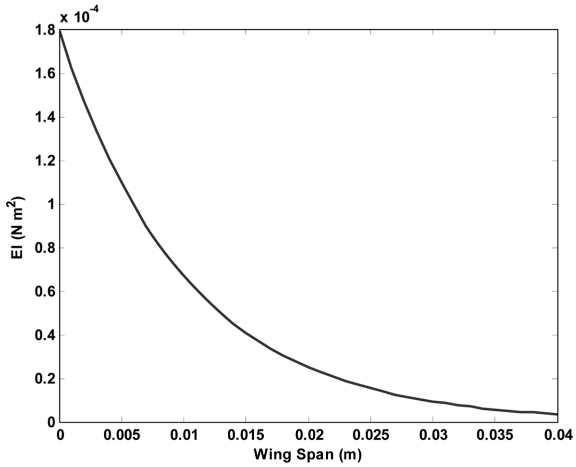

Fig. 16 Spanwise flexural stiffness distribution of dragonfly wing (Combes and Daniel 2003)

Average flexural stiffness is calculated, using Eq. (24), and subsequently used to obtain the static tip deflection of the *Aeshna Multicolor* wing using the beam equation

$$EI\frac{d^2w}{dX_1^2} = M \tag{26}$$

An equivalent beam model proposed by Lee *et al*. (2005) is used to calculate static tip deflection of the uniform IPMC flapping wing. This model is a grey box model and occupies a position between a physics based model and a black box model. Fig. 17 shows the comparison of the tip deflections of both wings due to a point force of 0.003 N applied at the tip (Combes and Daniel 2003). Average flexural stiffness of the dragonfly wing is 4.46×10^{-5} Nm^2 where as flexural stiffness of the uniform IPMC flapping wing is 3.37×10^{-6} Nm^2. Therefore, it can be seen from Fig. 17 that the IPMC flapping wing is structurally more flexible than the actual dragonfly wing. We should also note that the dragonfly wing is a passive structure because flight muscles are restricted to the wing base. Therefore, wing does not deflect much but is actuated from the root of the wing to generate flapping motion (Dudley 2000).

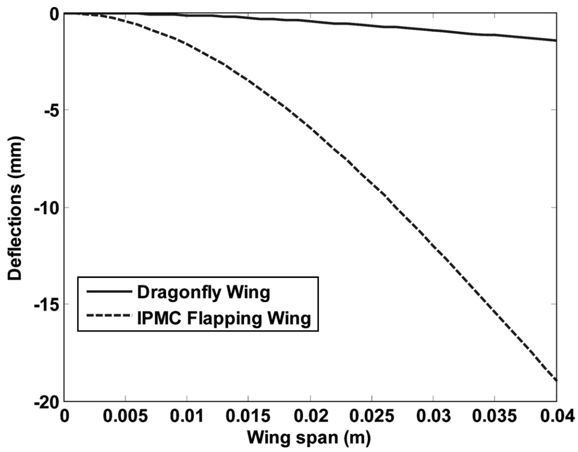

Fig. 17 Static tip deflection of dragonfly and IPMC wing

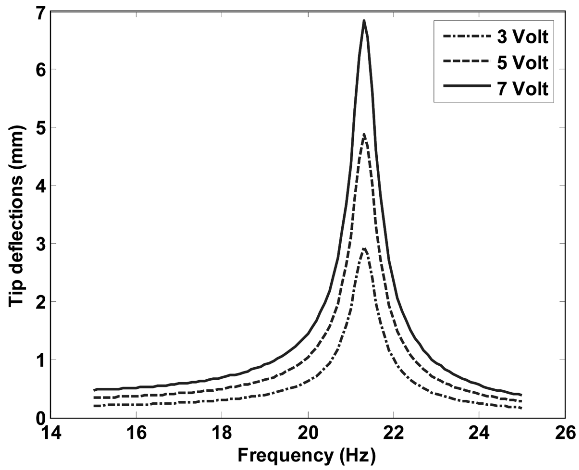

Fig. 18 Tip deflection of IPMC wing due to application of different voltages

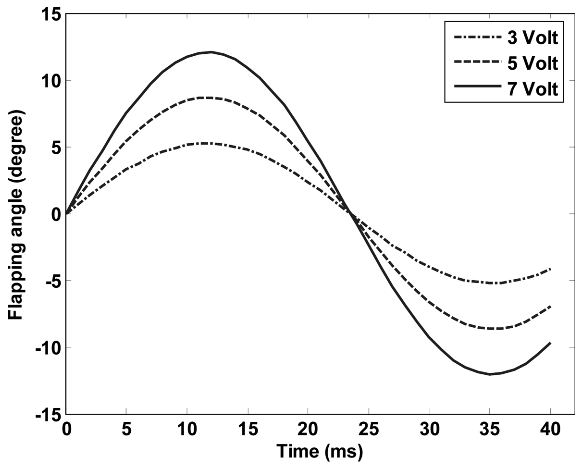

Fig. 19 Variation of the flapping angle of IPMC wing

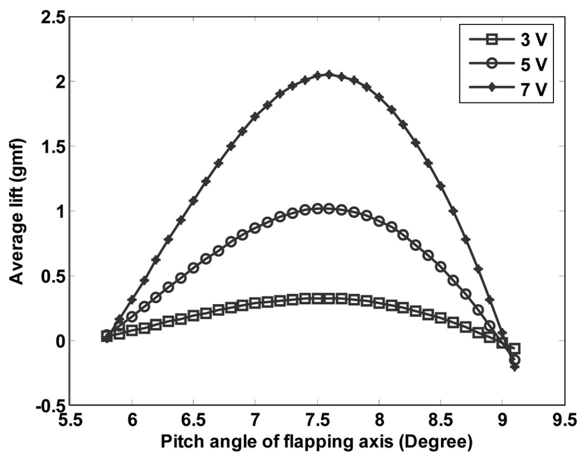

Fig. 20 Average lift at different pitch angle

However, IPMC wing creates the flapping motion through deflection. Fig. 18 shows the tip deflection of the IPMC flapping wing at different applied voltages. It can be seen from the Fig. 18 that maximum tip deflections of 6.84 mm is obtained when 7 volt is applied at 21 Hz. Variation of the flapping angle during the beating motion is shown in Fig. 19. Flapping angle of 12^0 is obtained at 7 volt.

For aerodynamic modeling, kinematics pertaining to the wing section located at 75% of the wing span is considered for calculation of the aerodynamic forces. Flapping angles of the wing section at that location are 3.6^0, 6^0 and 8^0 when actuated at 3 volt, 5 volt and 7 volt, respectively. Selection of the pitch angle of the flapping axis $\bar{\theta}_a$ is important for the performance of the flapping wing. Average lift pertaining to single wing at different pitch angle is shown in Fig. 20 when different voltages are applied. Fig. 21 shows the average thrust at different pitch angle and at different applied voltages. It can be seen from the Fig. 20 that the lift is maximum at the pitch angle of 7.5^0. However, at the pitch angle of 7.5^0, thrust which is same for all the three applied voltages has a negative value. Since average thrust force must be positive to satisfy the condition for cruise flight, therefore the value of $\bar{\theta}_a$ is selected as 6.5^0. Fig. 22 shows the average lift produced by the IPMC flapping wing at different flight speeds. It can be seen from the Fig. 22 that maximum lift force of 0.0063 N is obtained at 5 volt. It can also be

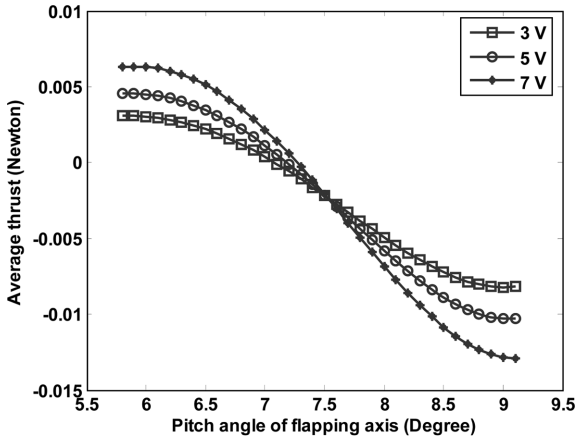

Fig. 21 Average thrust at different pitch angle

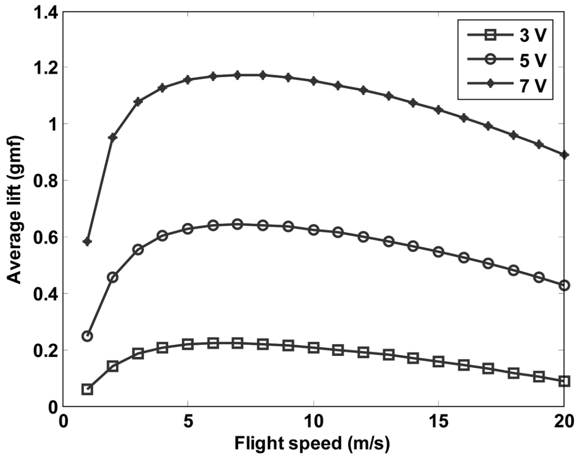

Fig. 22 Average lift at different flight speed

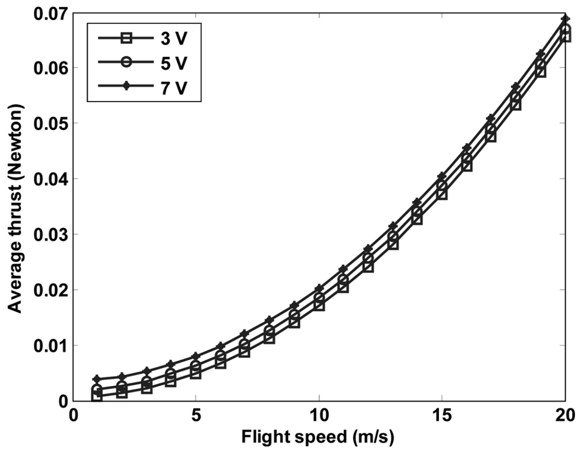

Fig. 23 Average thrust at different flight speed

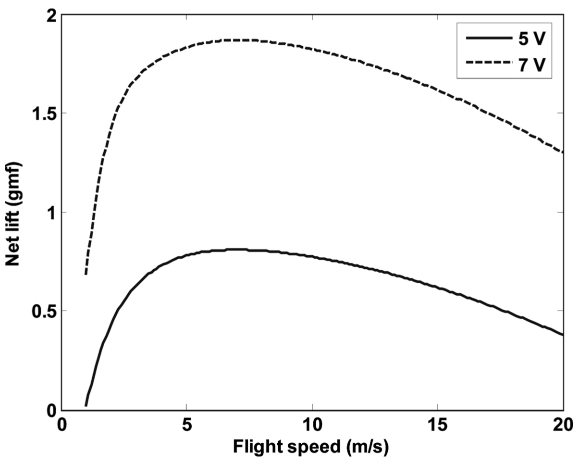

Fig. 24 Net lift at different flight speed

seen that the maximum lift force can reach up to 0.0115 N at 7 volt. In both the cases, maximum lift force occur at the flight speed of 7.1 m/s. Average thrust force at different flight speeds is shown in Fig. 23. The average thrust force is found to be 0.0122 N at the flight speed of 7.1 m/s when 7 volt is applied. Fig. 24 shows the net lift force, obtained by subtracting the total wing weight from the total lift force, when two IPMC flapping wings are used. It can be seen from the Fig. 24 that flapping wings can carry a payload of 1.87 g at 7 volt. We note that flapping performance of IPMCs in air degrades as the input voltage increases. However, substantial amount of research to obtain high performance IPMCs is going on (Kim and Kim 2008). It is expected that with further progress in IPMCs technology, it will become possible to obtain an IPMC flapping wing which may be actuated at a voltage higher than 7 volt. In order to be capable of autonomous flight, the flapping wing MAV requires several sub-systems such as power supply unit, control unit, sensory systems etc. These sub-systems can be made of light weight components such as thin sheet of solar cell, which can generate up to 20 $mW.cm^{-1}$, may be used for power supply unit (Deng *et al.* 2006, Tanaka *et al.* 2009). The net lift force generated by the IPMC flapping wing may be used to carry one or more of these sub-systems.

8. Conclusions

In this study, variational principle is used for dynamic modeling of the IPMC flapping wing. Dynamic characteristics of the wing are analyzed using numerical simulations. Design optimization is used to obtain improved performance of the flapping wing. The flapping angle of 12^0 is obtained at an input voltage of 7 volt at 21 Hz. An unsteady aerodynamic model is used to obtain the aerodynamic forces. The IPMC flapping wing can generate 0.0115 N average lift force at the flight speed of 7.1 m/s when 7 volt is applied. The average thrust force is found to be 0.0122 N at the same flight conditions. Moreover, it is possible to carry a payload of 1.87 g by using two IPMC flapping wings actuated at 7 volt, 21 Hz and flying at 7.1 m/s. The IPMC flapping wing may be considered as a potential candidate for use in MAV applications.

References

Akle, B.J., Bennett, M.D. and Leo, D.J. (2006), "High-strain ionomeric ionic liquid electroactive actuators", *Sensor. Actuat. A-Phys.*, **126**(1), 173-181.

Arora, J.S. (2004), *Introduction to optimum design,* 2nd Edition, Elsevier Academic Press, San Diego, California, USA.

Azuma, A., Azuma, S., Watanabe, I. and Furuta, T. (1985), "Flight mechanics of a dragonfly", *J. Exp. Biol.*, **116**(1), 79-107.

Bar-Cohen, Y. (Editor) (2004), *Electroactive Polymer (EAP) actuators as artificial muscles – Reality, potential, and challenges*, 2nd Edition, SPIE Press, Bellingham, Washington, USA.

Betteridge, D.S. and Archer, R.D. (1974), "A study of the mechanics of flapping wings", *Aeronaut. Q.*, **25**, 129-142.

Bohorquez, F., Samuel, P., Sirohi, J., Pines, D., Rudd, L. and Perel, R. (2003), "Design, analysis and hover performance of a rotary wing micro air vehicle", *J. Am. Helicopter Soc.*, **48**(2), 80-90.

Buechler, M.A. and Leo, D.J. (2007), "Characterization and variational modeling of ionic polymer transducers", *J. Vib. Acoust.*, **129**(1), 113-120.

Carrion, J.E. and Spencer, Jr. B.F. (2008), "Real-time hybrid testing using model-based delay compensation", *Smart Struct. Syst.*, **4**(6), 809-828.

Casciati, F. and van der Eijk, C. (2008), "Variability in mechanical properties and microstructure characterization of CuAlBe shape memory alloys for vibration mitigation", *Smart Struct. Syst.*, **4**(2), 103-121.

Combes, S.A. and Daniel, T.L. (2003), "Flexural stiffness in insect wings II. Spatial distribution and dynamic wing bending", *J. Exp. Biol.*, **206**(17), 2989-2997.

Cosyn, P. and Vierendeels, J. (2007), "Design of fixed wing micro air vehicles", *Aeronaut. J.*, **111**(1119), 315-326.

Cox, A., Monopoli, D., Cveticanin, D., Goldfarb, M. and Garcia, E. (2002), "The development of elastodynamic components for piezoelectrically actuated flapping micro-air vehicles", *J. Intel. Mat. Syst. Str.*, **13**(9), 611-615.

DeLaurier, J.D. (1993), "An aerodynamic model for flapping-wing flight", *Aeronaut. J.*, **97**(964), 125-130.

Deng, X., Schenato, L., Wu, W.C. and Sastry, S.S. (2006), "Flapping flight for biomimetic robotic insects: Part I - System modeling", *IEEE T. Robot.*, **22**(4), 776-788.

Dudley, R. (2000), *The biomechanics of insect flight - Form, function and evolution*, Princeton University Press, Princeton, New Jersey.

Grasmeyer, J.M. and Keennon, M.T. (2001), *Development of the black widow micro air vehicle*, *Fixed and Flapping Wing Aerodynamics for Micro Air Vehicle Applications* (Ed. T.J. Mueller), Progress in Astronautics and Aeronautics Series, AIAA, Reston, VA, USA.

Hein, B.R. and Chopra, I. (2007), "Hover performance of a micro air vehicle: Rotors at low Reynolds number", *J. Am. Helicopter Soc.*, **52**(3), 254-262.

Ke, S., Zhigang, W. and Chao, Y. (2008), "Analysis and flexible structural modeling for oscillating wing utilizing aeroelasticity", *Chin. J. Aeronaut.*, **21**(5), 402-410.

Kim, S.M. and Kim, K.J. (2008), "Palladium buffer-layered high performance Ionic Polymer-Metal Composites", *Smart Mater. Struct.*, **17**(6), 1363-1368.

Kim, J.M. and Koratkar, N. (2005), "Effect of unsteady blade pitching motion on aerodynamic performance of microrotorcraft", *J. Aircraft*, **42**(4), 874-881.

Liu, S.C. (2008), "Sensors, smart structures technology and steel structures", *Smart Struct. Syst.*, **4**(5), 517-530.

Lee, S., Park, H.C. and Kim, K.J. (2005), "Equivalent modeling for Ionic Polymer-Metal Composite actuators based on beam theories", *Smart Mater. Struct.*, **14**(6), 1363-1368.

Lee, S.G., Park, H.C. and Pandia, S.D. (2006), "Performance improvement of IPMC (Ionic Polymer Metal Composites) for a flapping actuator", *Int. J. Control Autom. Syst.*, **4**(6), 748-755.

Manna, M.C., Sheikh, A.H. and Bhattacharyya, R. (2009), "Static analysis of rubber components with piezoelectric patches using nonlinear finite element", *Smart Struct. Syst.*, **5**(1), 23-42.

McIntosh, S.H., Agrawal, S.K. and Khan, Z. (2006), "Design of a mechanism for biaxial rotation of a wing for a hovering vehicle", *IEEE-ASME T. Mech.*, **11**(2), 145-153.

Nelson, J. and Koratkar, N. (2005), "Effect of miniaturized gurney flaps on aerodynamic performance of microscale rotors", *J. Aircraft*, **42**(2), 557-561.

Okamoto, M. and Azuma, A. (2005), "Experimental study on aerodynamic characteristics of unsteady wings at low Reynolds number", *AIAA J.*, **43**(12), 2526-2536.

Park, H.C., Lee, S.K. and Kim, K.J. (2005a), "Equivalent modeling for shape design of IPMC (Ionic Polymer Metal Composite) as flapping actuator", *Key Eng. Mater.*, **297-300**, 616-621.

Park, S., Yun, C.B., Roh, Y. and Lee, J.J. (2005b), "Health monitoring of steel structures using impedance of thickness modes at PZT patches", *Smart Struct. Syst.*, **1**(4), 339-353.

Pines, D.J. and Bohorquez, F. (2006), "Challenges facing future micro-air-vehicle development", *J. Aircraft*, **43**(2), 290-305.

Ramasamy, M. and Leishman, J.G. (2006), "Phase-locked particle image velocimetry measurements of a flapping wing", *J. Aircraft*, **43**(6), 1867-1875.

Shahinpoor, M., Bar-Cohen, Y., Simpson, J.O. and Smith, J. (1998), "Ionic polymer-metal composites (IPMCs) as biomimetic sensors, actuators and artificial muscles - a review", *Smart Mater. Struct.*, **7**(6), R15-R30.

Shyy, W., Berg, M. and Ljungqvist, D. (1999), "Flapping and flexible wings for biological and micro air vehicles", *Prog. Aerosp. Sci.*, **35**(5), 455-505.

Singh, B. and Chopra, I. (2008), "Insect-based hover-capable flapping wings for micro air vehicles: Experiments and analysis", *AIAA J.*, **46**(9), 2115-2135.

Sirohi, J., Parsons, E. and Chopra, I. (2007), "Hover performance of a cycloidal rotor for a micro air vehicle", *J. Am. Helicopter Soc.*, **52**(3), 263-279.

Tanaka, K., Oonuki, M., Moritake, N. and Uchiki, H. (2009), "Cu_2ZnSnS_4 thin film solar cells prepared by non-vacuum processing", *Sol. Energ. Mat. Sol. C.*, **93**(5), 583-587.

Tarascio, M.J., Ramasamy, M., Chopra, I. and Leishman, J.G. (2005), "Flow visualization of micro air vehicle scaled insect-based flapping wings", *J. Aircraft*, **42**(2), 385-390.

Tiwari, R., Kim, K.J. and Kim, S.M. (2008), "Ionic polymer-metal composite as energy harvesters", *Smart Struct. Syst.*, **4**(5), 549-563.

Wakeling, J.M. and Ellington, C.P. (1997), "Dragonfly flight. I. Gliding flight and steady-state aerodynamic forces", *J. Exp. Biol.*, **200**(3), 543-556.

Wang, Z.J. (2000), "Vortex shedding and frequency selection in flapping flight", *J. Fluid Mech.*, **410**, 323-341.

Willmott, A.P. and Ellington, C.P. (1997), "The mechanics of flight in the hawkmoth Manduca sexta I. Kinematics of hovering and forward flight", *J. Exp. Biol.*, **200**(21), 2705-2722.

Wu, J.H. and Sun, M. (2004), "Unsteady aerodynamic forces of a flapping wing", *J. Exp. Biol.*, **207**(23), 1137-1150.

Yamamoto, M. and Isogai, K. (2005), "Measurement of unsteady fluid dynamics forces for a mechanical dragonfly model", *AIAA J.*, **43**(12), 2475-2480.

Ying, Z.G., Ni, Y.Q. and Ko, J.M. (2009), "A semi-active stochastic optimal control strategy for nonlinear structural systems with MR dampers", *Smart Struct. Syst.*, **5**(1), 69-79.

Zeng, L., Matsumoto, H. and Kawachi, K. (1996), "A fringe shadow method for measuring flapping angle and torsional angle of a dragonfly wing", *Meas. Sci. Technol.*, **7**(5), 776-781.

CC

Notations

a : Co-efficient of exponential equation
$\underline{A}$: Generalized coordinate of mechanical displacements
b : Width of IPMC flapping actuator
c : Airfoil chord
c_n : Normal force coefficient
$\mathbf{c^D}$: Stiffness matrix at constant electric displacement
C : Coefficient of exponential equation
$(C_d)_f$: Drag coefficient due to skin friction
$\mathbf{C^{-1}}$: Inverse of capacitance
d : Strain coefficient
$\underline{D}$: Electric displacement vector
$\underline{EI}$: Flexural stiffness
$\overline{EI}$: Average flexural stiffness of *Aeshna Multicolor* wing
$\underline{f}$: Force vector
$\bar{h}_t$: Thickness of IPMC flapping wing
$\mathbf{h}$: Electromechanical coupling matrix
j : Square root of -1
$\mathbf{K_s}$: Diagonal stiffness matrix
L : Wingspan of *Aeshna Multicolor*
L_f : Unsupported length of IPMC flapping wing
L_t : Total length of IPMC flapping wing
L_u : Differential operator
M : Bending moment
$\mathbf{M_s}$: Diagonal mass matrix
$\underline{q}$: Generalized coordinate of electric displacements
s : Laplace variables
$\underline{T}$: Stress vector
$\mathcal{T}$: Kinetic energy
U : Flight speed
v : Electric potential applied on each electrode
V : Relative velocity
V_x : Flow speed tangential to the section
$\mathcal{V}$: Potential energy
$\mathcal{V}_{se}$: Strain energy
$\mathcal{V}_{couple}$: Coupling potential energy
$\mathcal{V}_{dielectric}$: Dielectric potential energy
w : Deflection in X_3 direction
w_{tip} : Tip deflection of IPMC flapping wing
$\mathcal{W}^{ext}$: Work done by external force
X_i : Cartesian axes (i=1,2,3)
y : Coordinate along the semispan
α_0 : Angle of section's zero lift line
α' : The flows relative angle of attack at the ¾ chord location
β_n : Eigenvalues
δ : Variation
$\varepsilon^{\mathbf{T}}$: Dielectric permittivity matrix at constant stress
η_s : Leading edge suction efficiency
$\underline{\theta}$: Pitch angle of chord with respect to U
$\underline{\theta_a}$: Pitch angle of flapping axis with respect to U
$\overline{\theta_w}$: Mean pitch angle of chord with respect to flapping axis

ρ	: Density of IPMCs
ρ_{air}	: Atmospheric density
σ_n	: Constant
υ_2	: Mid-chord normal velocity component due to the wing's motion
$\underline{\Phi}_u$	: Mechanical shape functions
$\underline{\Phi}_D$	: Electrical shape functions
$\underline{\Psi}$	: Coupling vector
ω	: Frequency
$(\ )_{,xx}$	: Second derivative with respect to space
$(\ )_u$	: Upper bound for design optimization
$(\ )_l$	: Lower bound for design optimization